European Journal of
Mineralogy
Open Access

Iron oxidation state in serpentines and magnesian chlorites of subduction-related rocks

Bruno Reynard[1], Clémentine Fellah[1], and Catherine McCammon[2]

[1]Université de Lyon, ENSL, UCBL, CNRS, LGL-TPE, 69007 Lyon, France
[2]Bayerisches Geoinstitut, University of Bayreuth, 95447 Bayreuth, Germany

Correspondence: Bruno Reynard (bruno.reynard@ens-lyon.fr)

Abstract. The ferric iron content in hydrothermally altered ultrabasic rocks and their major minerals, serpentines and Mg-chlorites, is important for establishing the oxidation state budget from oceanic ridges to subduction zones, in carbonaceous chondrites, and for modeling phase equilibria. A compilation of literature Mössbauer spectroscopic data on serpentines and magnesian chlorites from high-pressure ophiolites yields much lower ferric-to-total-iron ratios (Fe^{3+} / Fe_{total}) than those obtained on similar samples by X-ray absorption near-edge spectroscopy (XANES), leading to contradictory estimates of the ferric iron budget of subduction zones. New Mössbauer analysis of antigorite and Mg-chlorite samples from suites of high-pressure ophiolitic terrains of various Phanerozoic ages confirms the low and homogeneous values previously obtained by this technique, while lizardite inherited from oceanic hydrothermal alteration is ferric iron rich. We argue that XANES values may be biased by photo-oxidation when samples have a high Mg content, which is the case for serpentines and chlorites from subduction zones. Photo-oxidation is less important in Fe-poor phyllosilicates of the mica and talc families and does not affect the Fe-rich serpentines (greenalite, cronstedtite) of meteorites or Fe-rich terrestrial phyllosilicates. Mössbauer Fe^{3+} / Fe_{total} ratios of serpentine confirm the occurrence of a major redox change at the lizardite–antigorite transition near 300–400 °C rather than at the dehydration of antigorite at 500–650 °C in serpentinites from high-pressure ophiolites.

1   Introduction

Serpentinites and related rocks form by hydration of ultrabasic and basic rocks at conditions ranging from those of the surface of the Earth (Etiope et al., 2011), ocean floor (Fruh-Green et al., 2004; Kelley et al., 2001) or Mars (Ehlmann et al., 2009) to those of depths of 150–200 km in subduction zones (Ulmer and Trommsdorff, 1995). Serpentinization is associated with redox reactions affecting iron in hydrous silicates and carbon in fluids, resulting in hydrogen and hydrocarbon production (Andreani et al., 2013) and providing potential niches for early life (Pons et al., 2011; Schulte et al., 2006). Deeper in subduction zones, redox reactions can affect the nature of carbon-bearing phases in association with serpentinization (Vitale Brovarone et al., 2017), providing deep fluid sources of reduced carbon to feed a deep biosphere (Vitale Brovarone et al., 2020). In carbonaceous chondrites, knowledge of the redox state of iron in hydrous silicates is essential for understanding hydrothermal reactions and their relationship to the evolution of organics and carbonaceous matter (Beck et al., 2012; Garenne et al., 2019).

Measurement of the ferric-to-total-iron ratio is essential in quantifying redox processes and relies either on bulk rock composition measurement (Padrón-Navarta et al., 2011; Evans, 2012) or on spectroscopic determination in mineral fractions and modal composition of rocks (Debret et al., 2014, 2015). Conventional Mössbauer spectroscopy has been widely applied for decades but has a resolution no better than a few hundred micrometers, which restricts imaging and mapping (McCammon et al., 1991; Sobolev et al., 1999), a possibility offered by X-ray absorption near-edge spectroscopy (XANES) to within a few micrometers or less (Wilke et al., 2001). Thus, Mössbauer spectroscopy can be applied reliably to rocks with homogeneous mineralogical composition (Fig. 1a) and to separated mineral frac-
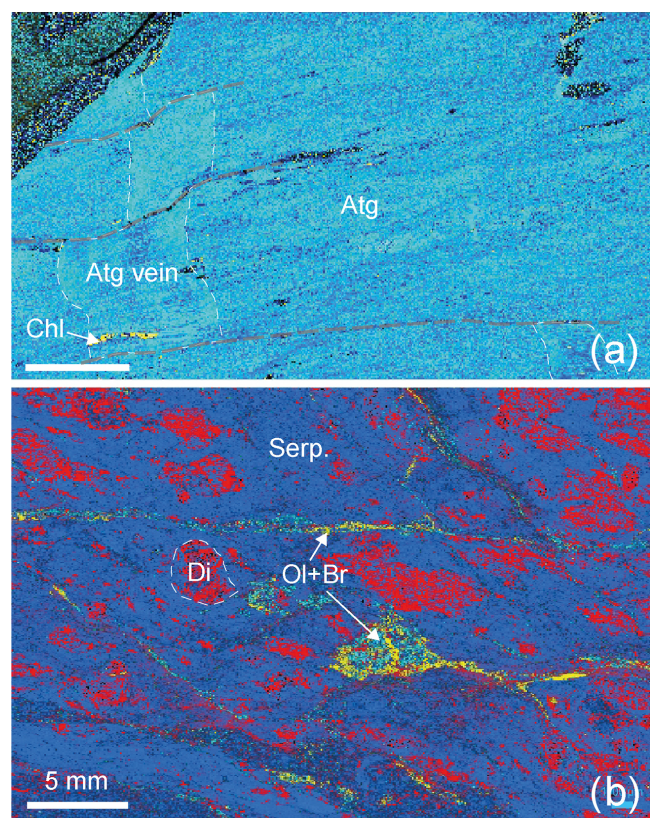
Figure 1. Raman maps of thin sections from high-pressure serpentinites of the Monviso area, Western Alps. **(a)** Foliated antigorite schists (sample Viso4) of nearly monomineralic composition (antigorite (Atg): blue; minor chlorite (Chl): yellow; glass slide: black), with antigorite veins (dashed white lines) cross-cutting the foliation and shifted by late minor fractures (dashed grey lines). Variations in the blue tone correspond to variations in crystal orientation and highlight the rock texture. **(b)** Weakly deformed serpentinite (Viso6) with complex mineralogy and texture partly preserved from the oceanic history, with former clinopyroxenes partly replaced by metamorphic diopside (Di) and chlorite, in a matrix of serpentine (Serp.), and olivine–brucite patches and veins (Ol + Br).

and estimate redox changes associated with reactions involving serpentine transformation and destabilization. We discuss the relative merits of Mössbauer and XANES for quantifying ferric-to-total-iron ratios in ferro-magnesian phyllosilicates from terrestrial rocks and meteorites.

2 Samples

The samples come from ophiolites and tectonic mélange units of Cenozoic to Paleozoic age. Samples from the Alps are similar in nature to those previously studied by XANES (Debret et al., 2014) as they come from similar high-pressure oceanic units that suffered subduction-type blueschist–eclogite facies metamorphic conditions of about 1.5–2.5 GPa and 450–600 °C during the Eocene (Scambelluri et al., 1997; Schwartz et al., 2013). Samples from Baja California Sur belong to the basal serpentinite unit of the Sierra de San Andrés ophiolite, Vizcaíno Peninsula, Mexico (Sedlock, 2003). This mélange comprises tectonic blocks that were metamorphosed under conditions ranging from pumpellyite to blueschist facies at 200–500 °C and 0.3–0.8 GPa ca. 180 Myr ago (Moore, 1986). The Ōeyama sample comes from a mélange complex that was metamorphosed under pumpellyite to high epidote–blueschist facies up to 450–550 °C and 1.5 GPa ca. 320 Myr ago (Tsujimori and Itaya, 1999).

Minerals were extracted from five serpentinites and two chloritites. Rocks that present a nearly monomineralic composition or large crystals of lizardite in bastite texture were carefully chosen in order to obtain single mineral separates in the required quantity (about 200 mg) for Mössbauer spectroscopy. Sample mineralogy (Table 1) was checked by optical microscopy and Raman spectroscopy (Reynard et al., 2015; Schwartz et al., 2013) on thin or thick sections and on separated and extracted powders.

Scanning electron microscopy and energy-dispersive X-ray (SEM-EDX) analyses were performed only on thin and thick sections. Sample sections were coated with a 20 nm thick carbon layer for analysis (Table 1) with EDX analysis using an AZtec Oxford Instruments system (DDI detector X-Max) installed on a Zeiss Supra VP55 scanning electron microscope operated at 15 kV and in high vacuum, except for sample ZS24, which was analyzed by electron microprobe (Masci et al., 2019). Chlorite and serpentine composition is homogeneous on the micrometer scale, except in BCS16B, where slight zoning causes a higher variability in the Mg and Si contents than in other samples.

Lizardite was extracted from bastite textures of a preserved oceanic serpentinite of Baja California Sur (BCS32), where topotactic replacement of original pyroxene produced lizardite crystals with grain sizes of a few millimeters. SEM showed these grains to contain minor tiny metallic inclusions (<0.1 % in volume) and magnetite (<1 % in volume).

tions, while XANES allows the study of complex mineralogy (Fig. 1b), a common case in natural rocks.

Applications of XANES spectroscopy to ferro-magnesian phyllosilicates include chlorites (Muñoz et al., 2006), talc, micas and serpentine minerals (Muñoz et al., 2013). However, antigorites display XANES-determined ferric iron contents (Debret et al., 2014, 2015; Muñoz et al., 2013) that are much higher than those obtained from Mössbauer spectroscopy on samples from similar geological settings (Evans et al., 2012). Wet-chemistry determinations of ferric-to-total-iron ratios in hydrated ultramafic rocks are also questionable as Mössbauer and chemical measurements yield discrepant results (Rozenson et al., 1979).

Here we investigate several antigorite and chlorite samples from high-pressure ophiolites using Mössbauer spectroscopy

Table 1. Chemical composition and mineralogical mode of samples analyzed by Mössbauer spectroscopy.

Sample	BCS32	BCS16A	Ōeyama	ET5	Viso4 matrix	Viso4 vein	ZS24	BCS6F
	Liz[1]	Atg[2]	Atg[2]	Atg[2]	Atg[2]	Atg[2]	Chl[3]	Chl[3]
n	10	11	8	8	9	10	6	16
M sites								
Mg	5.46(6)	5.16(10)	5.34(8)	5.26(6)	5.06(6)	5.06(6)	4.45(2)	2.99(2)
Fe_{total}	0.44(4)	0.32(4)	0.16(4)	0.28(4)	0.42(2)	0.42(2)	0.44(1)	1.78(2)
Al	0.08	0.06	0.04	0.02	0.1	0.1	0.97	1.09
□	0.02	0.04	0.04	0.02	–	–	0.14	0.14
Fe^{3+} / Fe_{total}	0.49(5)	0.23(4)	0.21(4)	0.22(3)	0.17(3)	0.22(3)	0.26(4)	0.13(3)
T sites								
Al	0.26	0.08	0.08	0.1	0.16	0.16	0.83	1.01
Si	3.74(4)	3.92(12)	3.92(8)	3.90(4)	3.84(1)	3.84(1)	3.17(2)	2.99(3)
Al_{total}	0.34(4)	0.14(8)	0.14(4)	0.12(2)	0.26(2)	0.26(2)	1.80(3)	2.10(2)
Serpentine	>99 %	>99 %	>99 %	>99 %	>99 %	>99 %	–	–
Chlorite	–	–	–	–	–	–	>98 %	~98 %
Titanite	–	–	–	–	–	–	–	~2 %
Magnetite	–	–	–	–	–	–	<2 %	–

[1] Lizardite: $M_6T_4O_{10}(OH)_8$. [2] Antigorite: $M_{5.58}T_4O_{10}(OH)_{7.04}$ assuming $m = 14$ modulation. [3] Chlorite: $M_6T_4O_{10}(OH)_8$; estimated standard deviation for total Mg, Fe, Al and Si based on n analyses; $Fe^{3+} / \Sigma Fe$ ratios from present Mössbauer data.

Antigorites were obtained from a foliated serpentinite of Baja California Sur (BCS16A); from an antigorite vein in a serpentinite of the Erro–Tobbio massif, Western Alps (ET5); and from the Monviso massif, Western Alps (Viso4), which comprised two subsamples from the foliated matrix and from a cross-cutting vein. Raman mapping demonstrated a nearly pure antigorite composition and showed structural relationships between veins and foliation (Fig. 1a). In these samples, the main impurity is magnetite (<5 %) and sometimes chlorite (<1 %). Another sample from the same area showed more complex mineralogy partly inherited from oceanic metamorphism and was therefore not considered for bulk Mössbauer analysis (Viso6, Fig. 1b) but could meaningfully be analyzed by high-resolution XANES mapping. Antigorite from a foliated serpentinite of the Ōeyama massif does not contain magnetite but does contain trace amounts of pentlandite (<0.1 %). These homogeneous serpentinite samples contained no olivine or pyroxene.

The two studied chlorites were a Si-rich clinochlore (penninite) extracted from a foliated chloritite (ZS24) from the Zermatt–Saas zone of the Western Alps and a ferrous clinochlore (pycnochlorite) extracted from a foliated chloritite (BCS6F) from Baja California Sur. Magnetite is the main impurity in ZS24 and titanite (~ 2 %) or clinopyroxene (<1 %) the main one in the BCS6F sample.

3 Mössbauer analyses

The oxidation state of iron was determined using Mössbauer spectroscopy. Extracted samples were gently crushed in alcohol in an agate mortar, and the magnetic fraction was removed by dipping a magnet into the powdered sample. An aliquot of 200 mg powder of each sample was loaded into a plastic holder with 12 mm diameter, giving a Mössbauer thickness between 3 and 8 mg Fe cm^{-2}, except for BCS6F chlorite, which has a thickness of 29 mg Fe cm^{-2} due to its higher Fe content. Spectra were recorded at room temperature in transmission mode on a constant acceleration Mössbauer spectrometer with a nominal 1.85 GBq ^{57}Co source in a 6 μm Rh matrix where the velocity scale was calibrated relative to α-Fe foil. We collected all spectra at ± 5 mm s^{-1} and additionally at ± 12 mm s^{-1} when magnetite peaks were present (ZS24 chlorite). Each spectrum was collected for 2–4 d, except for BCS32 lizardite (5 h) and the Viso4 antigorite vein (12 d).

Mössbauer spectra (Fig. 2) were fit using MossA software (Prescher et al., 2012) in the thin absorber approximation and additionally using the full transmission integral for thick samples (e.g., BCS6F chlorite). We used pseudo-Voigt line shapes to account for next-nearest-neighbor effects and variable area ratios for doublet components to account for preferred orientation. Hyperfine parameters (Table 2) are consistent with literature values for serpentine (Evans et al., 2012). Magnetite was detected in ZS24 by its characteristic sextets (Fig. 2g) that were constrained based on a spectrum collected
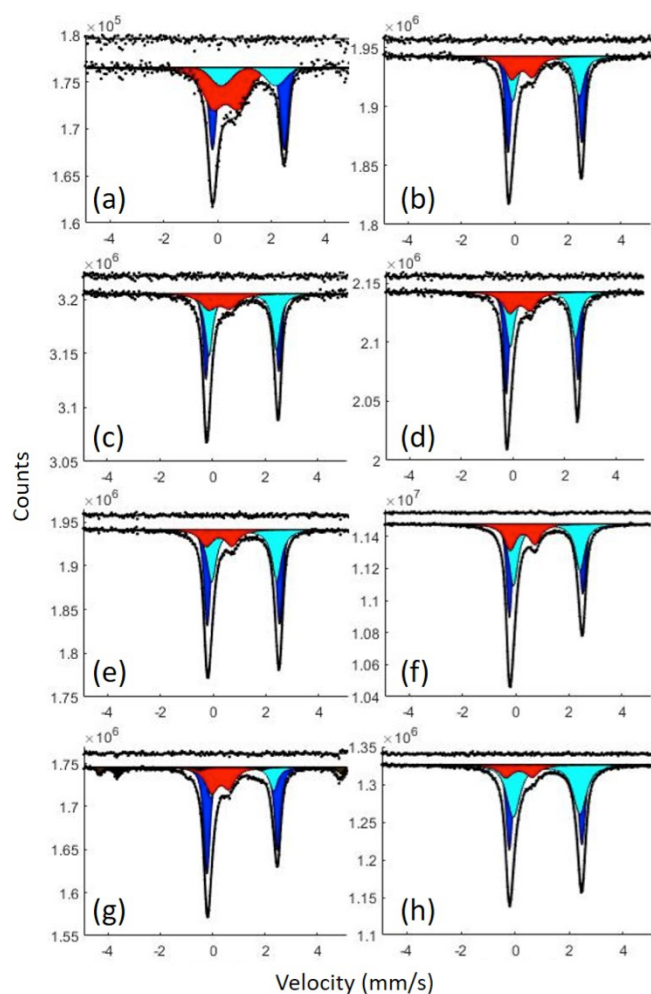
Figure 2. Room temperature Mössbauer spectra of serpentines and chlorites: **(a)** BCS32, **(b)** BCS16A, **(c)** Ōeyama, **(d)** ET5, **(e)** Viso4 matrix, **(f)** Viso4 vein, **(g)** ZS24 and **(h)** BCS6F. All spectra were fit with two doublets assigned to Fe^{2+} (dark blue and light blue) and one doublet assigned to Fe^{3+} (red). The spectrum from chlorite ZS24 **(g)** was additionally fit to two sextets assigned to magnetite (black) that were constrained based on a spectrum collected of the same sample at $\pm 12\,\mathrm{mm\,s^{-1}}$.

of the same sample at $\pm 12\,\mathrm{mm\,s^{-1}}$. Ferric-to-total-iron ratios were calculated from the relative areas of subspectra.

Values were not corrected for differences in the recoil-free fraction, since such differences have been shown to be minimal when ferrous and ferric iron occupy sites with similar coordination (e.g., Rancourt et al., 1994; Piilonen et al., 2004). Thickness effects can be neglected, since fits using the full transmission integral gave nearly identical results to fits using the thin absorber approximation. Magnetite absorption does not overlap chlorite absorption and does not affect ferric iron determination. The Mössbauer spectrum of titanite overlaps ferric iron absorption in serpentine (Muir et al., 1984),

so the ferric-to-total-iron ratio of BCS6F is likely overestimated by 1 %–2 %.

Antigorites have a remarkably constant ferric-to-total-iron ratio in the range 0.17(3)–0.23(4), in spite of the different pressure–temperature metamorphic conditions and ages of formation (Tables 1 and 2). The matrix antigorite Viso4 gives the lowest value, while all other antigorite values are the same within error bars with a mean value of 0.22(3). BCS32 lizardite gives a ferric-to-total-iron ratio of 0.49(5); Fe-rich clinochlore BCS6F and Mg-rich chlorite ZS24 give values of 0.13(3) and 0.26(3), respectively.

4 Discussion

A compilation of determinations of Fe^{3+} / Fe_{total} ratios in serpentines and Mg-rich chlorites with $X_{Fe} < 0.2$ by Mössbauer spectroscopy (Aja and Dyar, 2002; Bertoldi et al., 2001; Billault et al., 2002; De Grave et al., 1987; Evans et al., 2012; Fuchs et al., 1998; Goodman and Bain, 1979; Gregori and Mercader, 1994; Lougear et al., 2000; Malmström et al., 1996; Mellini et al., 2002; Mitra and Bidyananda, 2001; O'Hanley and Dyar, 1993, 1998; Peretti et al., 1992; Rozenson et al., 1979; Smyth et al., 1997; Votyakov et al., 2005; Zazzi et al., 2006), the present data and XANES (Andreani et al., 2013; Debret et al., 2014, 2015; Masci et al., 2019; Muñoz et al., 2013; Rigault, 2010; Trincal et al., 2015; Vidal et al., 2006) reveals important trends (Fig. 3).

Box plots and histograms emphasize the large overlap of Fe^{3+} / Fe_{total} ratios from XANES and Mössbauer data in lizardite and a small overlap of XANES and Mössbauer data in antigorite. For chlorites, overlap between XANES and Mössbauer data is larger than in antigorites. Mössbauer analyses show higher ferric iron content ($Fe^{3+} / Fe_{total} > 0.3$) where secondary continental alteration by meteoritic waters was inferred for lizardites (Votyakov et al., 2005) and is supposed for antigorite and chlorite populations, as discussed in Sect. 4.1. Mean values, standard errors, standard deviations and median values are reported in Table 3 for all populations.

Typically, uncertainties in the means (2 SE, Table 3) are lower than 10 % and often lower than 5 %. Standard deviations pertinent to individual analyses are lower than 10 % for Mössbauer analyses of antigorites and chlorites and 20 % for XANES and Mössbauer data of lizardites.

4.1 Mössbauer data

Mössbauer analyses of lizardites can be separated into two groups, one defined by a single extensive study (74 analyses) of serpentinized ultramafic rocks of the Ural Mountains (Votyakov et al., 2005) and the other comprising about 40 analyses (Evans et al., 2012; O'Hanley and Dyar, 1993; Rozenson et al., 1979; Fuchs et al., 1998). Serpentinization in the Ural subgroup is inferred to have been caused by meteoritic waters in a continental setting (Votyakov et

Table 2. Hyperfine parameters derived from room temperature Mössbauer spectra of serpentines and chlorites.

	BCS32	BCS16A	Ōeyama	ET5	Viso4 (m)	Viso4 (v)	ZS24	BCS6F
Fe^{2+} (I) silicate								
CS ($\mathrm{mm\,s^{-1}}$)	1.15(1)	1.14(1)	1.14(1)	1.14(1)	1.15(1)	1.14(1)	1.13(1)	1.14(1)
QS ($\mathrm{mm\,s^{-1}}$)	2.67(2)	2.75(2)	2.78(4)	2.76(2)	2.74(2)	2.75(1)	2.69(3)	2.68(1)
FWHM ($\mathrm{mm\,s^{-1}}$)	0.35(7)	0.28(3)	0.26(4)	0.25(2)	0.29(2)	0.27(1)	0.30(2)	0.29(2)
Area	0.34(25)	0.43(14)	0.38(21)	0.41(11)	0.42(7)	0.35(5)	0.40(10)	0.37(9)
Area ratio $1:2$[1]	1	1.11(1)	1.10(1)	1.17(1)	1.02(1)	1.33(1)	1.28(1)	1.07(1)
Fe^{2+} (II) silicate								
CS ($\mathrm{mm\,s^{-1}}$)	1.15(1)	1.17(4)	1.16(1)	1.17(2)	1.18(1)	1.17(1)	1.12(3)	1.17(1)
QS ($\mathrm{mm\,s^{-1}}$)	2.02(92)	2.50(12)	2.57(13)	2.52(9)	2.47(7)	2.50(3)	2.39(16)	2.46(6)
FWHM ($\mathrm{mm\,s^{-1}}$)	0.86(48)	0.43(9)	0.35(8)	0.38(7)	0.43(5)	0.42(2)	0.39(10)	0.59(3)
Area	0.17(27)	0.34(15)	0.41(21)	0.37(12)	0.40(7)	0.43(4)	0.17(11)	0.50(9)
Fe^{3+} silicate								
CS ($\mathrm{mm\,s^{-1}}$)	0.30(7)	0.28(11)	0.27(9)	0.28(8)	0.23(4)	0.26(2)	0.29(6)	0.15(2)
QS ($\mathrm{mm\,s^{-1}}$)	0.95(9)	0.78(22)	0.81(16)	0.79(14)	0.98(8)	0.93(4)	0.66(10)	0.98(7)
FWHM ($\mathrm{mm\,s^{-1}}$)	0.94(11)	0.61(9)	0.76(14)	0.64(9)	0.59(8)	0.53(3)	0.59(8)	0.61(9)
Area	0.49(5)	0.23(4)	0.21(4)	0.22(3)	0.17(3)	0.22(2)	0.20(4)	0.13(3)
$Fe^{2.5+}$ magnetite[2]								
CS ($\mathrm{mm\,s^{-1}}$)							0.67(2)	
ε ($\mathrm{mm\,s^{-1}}$)							0.01(3)	
B (T)							45.9(1)	
FWHM ($\mathrm{mm\,s^{-1}}$)							0.37(5)	
Area							0.15(4)	
Fe^{3+} magnetite[2]								
CS ($\mathrm{mm\,s^{-1}}$)							0.28(2)	
ε ($\mathrm{mm\,s^{-1}}$)							0.01(3)	
B (T)							49.2(1)	
FWHM ($\mathrm{mm\,s^{-1}}$)							0.33(4)	
Area							0.07(3)	

Abbreviations: CS – center shift relative to α-Fe, QS – quadrupole splitting, FWHM – full width at half maximum, ε – quadrupole shift, B – hyperfine magnetic field, v – vein, m – matrix. [1] The area ratio of doublet components was allowed to vary to account for preferred orientation but constrained to have the same value for all silicate doublets according to symmetry. [2] Based on spectrum recorded with velocity range -12 to $+12\,\mathrm{mm\,s^{-1}}$.

Table 3. Statistical parameters of Fe^{3+}/Fe_{total} ratios in serpentine and low-Fe chlorite mineral populations.

	Mössbauer										XANES		
	Lizardite			Chrysotile	Antigorite			Chlorites			Lizard.	Antig.	Chlorite
	All	1	2		All	1	2	All	1	2			
Mean	0.67	0.59	0.71	0.34	0.23	0.16	0.39	0.30	0.15	0.49	0.71	0.64	0.51
2 SE	0.03	0.07	0.02	0.06	0.03	0.02	0.03	0.08	0.05	0.05	0.06	0.08	0.10
σ	0.17	0.24	0.10	0.12	0.10	0.06	0.05	0.10	0.08	0.08	0.20	0.19	0.21
Median	0.72	0.57	0.72	0.32	0.21	0.16	0.40	0.27	0.12	0.49	0.76	0.66	0.50

SE: standard error; σ: standard deviation; 1: samples with primary metamorphic signature; 2: samples with secondary oxidation.
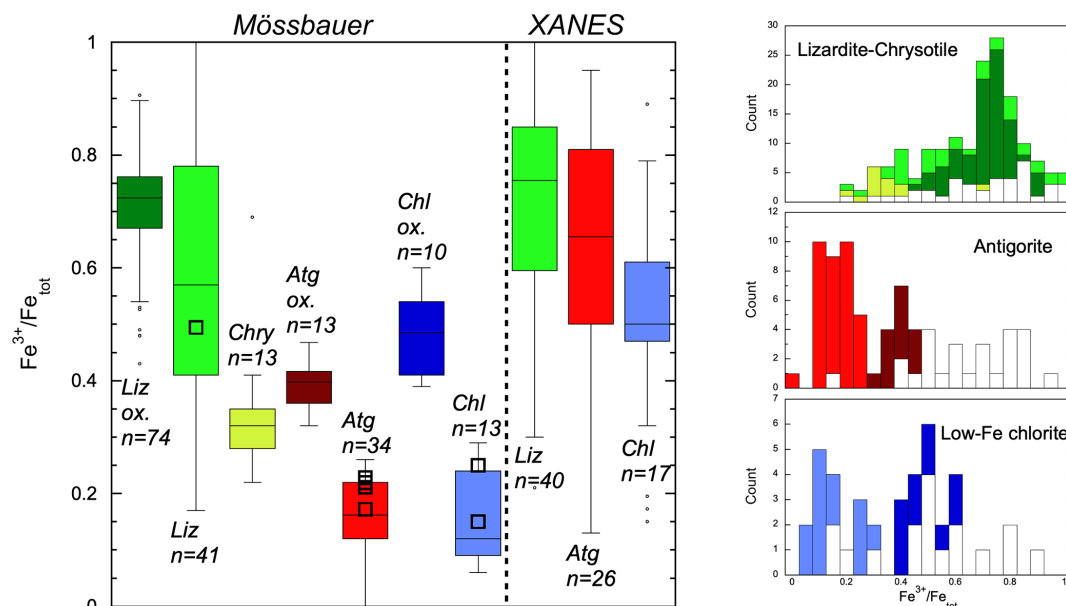
Figure 3. Determinations of Fe^{3+}/Fe_{total} ratios in serpentines and Fe-poor chlorites with $X_{Fe} < 0.2$ by Mössbauer and XANES. Liz: lizardites; Atg: antigorites; Chry: chrysotiles; Chl: chlorites. Darker tones are used for populations of samples that were oxidized (ox.) by secondary, likely continental, alteration. The number (n) of analyses is indicated for each box. Present data are shown as black squares. Corresponding histograms for lizardite (and chrysotile), antigorite and chlorite are shown on the left (XANES data in white, Mössbauer in color).

al., 2005), while the other analyses refer mostly to serpentines formed during oceanic floor hydrothermal alteration. The two groups display a broad range of values. The Ural lizardites show higher and less dispersed values than those of oceanic lizardites with mean ratios of 0.71(2) and 0.59(7), respectively (number in parentheses is the uncertainty in the mean value last digit, estimated as 2 standard errors).

Mössbauer analyses of antigorites display much lower Fe^{3+}/Fe_{total} ratios than lizardites, with a mean value of 0.23(3) (Evans et al., 2012; Mellini et al., 2002; Peretti et al., 1992; Rozenson et al., 1979; Votyakov et al., 2005). The population is bimodal, with one subgroup characterized by Fe^{3+}/Fe_{total} values above 0.32 with a mean value of 0.39(3) dominated by samples (9 out of 13) from the Ural ultramafics (Votyakov et al., 2005) and one characterized by Fe^{3+}/Fe_{total} values below 0.26 with a mean value of 0.16(2) dominated by samples from high-pressure ophiolites. We interpret the low values as pristine records of Fe^{3+}/Fe_{total} ratios for high-pressure metamorphic antigorites to which all samples measured here belong, while the high values may reflect oxidation due to secondary continental alteration by meteoritic waters that was shown to affect serpentinites in the Ural ultramafics (Votyakov et al., 2005). Finally, chrysotile samples display intermediate values between antigorites and lizardites, with a mean value of 0.34(6) (O'Hanley and Dyar, 1998).

Mössbauer analyses of Mg-rich chlorites ($X_{Fe} < 0.2$) yield Fe^{3+}/Fe_{total} ratios similar to those of antigorites, with a

mean value of 0.27(18). Two populations are identified, one with Fe^{3+}/Fe_{total} ratios above 0.4 and an average of 0.49(8) (Billault et al., 2002; Goodman and Bain, 1979; Malmström et al., 1996; Smyth et al., 1997) and one with Fe^{3+}/Fe_{total} ratios below 0.3 and an average of 0.15(8) (Aja and Dyar, 2002; Bertoldi et al., 2001; Gregori and Mercader, 1994; Lougear et al., 2000; Mitra and Bidyananda, 2001; Zazzi et al., 2006). By analogy with serpentine, the group with the highest values that contains samples of continental low-temperature hydrothermal origin (Billault et al., 2002) is attributed to oxidizing conditions during continental weathering, and the group with the lowest values is attributed to pristine compositions of high-pressure rocks.

The essentially constant values for antigorites and Mg-chlorites suggest that the Fe^{3+}/Fe_{total} ratio is controlled more by crystal chemistry than oxygen fugacity (fO_2) in the nearly monomineralic samples studied here. The limited effect of fO_2 on the Fe^{3+}/Fe_{total} ratio during high-pressure and mid- to high-temperature (400–700 °C) metamorphism is in line with petrological analysis that suggested controls by silica and alumina potential rather than or in addition to fO_2 (Chernosky et al., 1988; Evans et al., 2012). The large variation in Fe^{3+}/Fe_{total} ratios in lizardites suggests variable fO_2 or silica/alumina potential conditions during low-temperature metamorphism and oceanic hydrothermal alteration.

4.2 XANES data

XANES analyses of lizardites have been reported for oceanic serpentinites (Andreani et al., 2013) and for one suite of serpentinites from high-pressure ophiolites from the Western Alps (Debret et al., 2014). Antigorites were analyzed from the same suite of samples (Debret et al., 2014) and across the antigorite serpentinite dehydration sequence to chlorite peridotite, along with Mg-rich chlorite (Debret et al., 2015), in samples from the Cerro del Almirez (Padrón-Navarta et al., 2011). Lizardites display Fe^{3+} / Fe_{total} ratios of 0.71(20), which are higher than average but within the large range of observed values from Mössbauer spectroscopy. Fe^{3+} / Fe_{total} ratios for antigorites (Debret et al., 2014, 2015; Muñoz et al., 2013) and magnesian chlorites (Debret et al., 2015; Muñoz et al., 2013; Rigault, 2010) are systematically higher than the Mössbauer values, with averages of 0.63(19) for antigorite and 0.58(12) for magnesian chlorites, a discrepancy of 40 % that needs to be resolved. A study of orientation effects yielded high Fe^{3+} / Fe_{total} ratios (>0.8) on oriented antigorite fibers from a vein and low values (<0.3) on Mg-rich chlorite, talc and phlogopite (Muñoz et al., 2013). Orientation effects cause variations of $\pm 10\%$ around the average value (Muñoz et al., 2013) and cannot account for the 40 % discrepancy. Nor can uncertainties in the calibration, estimated to be about 10 % from the figures of the original study (Wilke et al., 2001) and subsequent applications to serpentines and chlorites (Andreani et al., 2013; Debret et al., 2014, 2015; Muñoz et al., 2013), account for this. Similar combined uncertainties of 10 %–15 % were obtained based on single-crystal studies of micas (Dyar et al., 2002). Orientation effects on pre-edge intensities were shown to be more important in pyroxenes (Dyar et al., 2002; Steven et al., 2022).

The difference between mean values of Fe^{3+} / Fe_{total} ratios obtained from XANES and Mössbauer spectroscopy on Mg-rich serpentines and chlorites is provisionally related to oxidation caused by the intense synchrotron X-ray beam in hydrous minerals, as already demonstrated in hydrous glasses (Cottrell et al., 2018). XANES determinations on Fe-rich chlorites (Masci et al., 2019; Rigault, 2010; Trincal et al., 2015; Vidal et al., 2006) yield Fe^{3+} / Fe_{total} ratios covering values down to zero (Fig. 4), in good agreement with Mössbauer determinations on Fe-rich chlorites (Aja and Dyar, 2002; Bertoldi et al., 2001; De Grave et al., 1987; Goodman and Bain, 1979; Gregori and Mercader, 1994; Lougear et al., 2000). This suggests little if any photo-oxidation in Fe-rich samples. Low Fe^{3+} / Fe_{total} ratios are also determined from XANES analyses of anhydrous silicates, in agreement with Mössbauer results when available (Wilke et al., 2001). Photo-oxidation thus appears to be limited to Mg-rich hydrous phases. Notable exceptions are one clinochlore sample, talc and phlogopite (Muñoz et al., 2013), which will be discussed below. Negligible photo-oxidation in serpentines during XANES was inferred from comparison of spectra af-

ter several minutes to several tens of minutes of irradiation (Andreani et al., 2013), but oxidation during the first seconds of XANES data acquisition because of the high brilliance of synchrotron beams cannot be excluded.

4.3 Photo-oxidation

In order to test the photo-oxidation hypothesis, we built a model with the following assumptions: (1) photo-oxidation occurs irreversibly on Fe^{2+} sites by removing the H atom of the OH ligand in the octahedral layers to compensate for the loss of an electron of the excited iron atom; (2) photo-oxidation occurs on Fe^{2+} sites that are isolated from each other by Mg atoms on the neighboring octahedral sites – it does not occur when one of the neighboring octahedral atoms is iron because the electron may be exchanged through electrical conduction by the small polaron mechanism active in phyllosilicates (Reynard et al., 2011); and (3) Fe, Mg and other cations are disordered on octahedral sites. With these assumptions, the fraction of isolated Fe^{2+} ions that may oxidize during XANES measurements is defined by the probability P of having six Mg or Al atoms on the six neighboring octahedral sites in a random distribution:

$$P = (1 - X_{Fe})^6. \tag{1}$$

Out of the Fe atoms, a fraction I was already in the Fe^{3+} state in the pristine sample; the final ferric iron fraction F after photo-oxidation is

$$F = (1 - I) \cdot P + I. \tag{2}$$

Curves showing the expected Fe^{3+} / Fe_{total} ratio after photo-oxidation using these relations are displayed in Fig. 4. At low X_{Fe}, the number of isolated Fe sites becomes significant, and the curves converge to F values of 1 when X_{Fe} tends to zero, accounting for high oxidation at low Fe content levels. As X_{Fe} reaches a value of ~ 0.3, F tends to I, and photo-oxidation is negligible (within the estimated uncertainty of 0.1 for XANES).

If the model is correct, XANES analysis should plot close to or above those curves, which is the case for a large fraction of lizardites and antigorite and Mg-chlorite XANES analyses (Fig. 4). A test sample is the ZS24 chlorite, for which both XANES (Masci et al., 2019) and Mössbauer (this study) data were obtained. Mössbauer analysis of sample ZS24 (this study) gives a Fe^{3+} / Fe_{total} ratio of 0.26(4), which, combined with X_{Fe} of 0.075(2), yields an expected Fe^{3+} / Fe_{total} ratio after photo-oxidation of 0.73(5), in agreement with the XANES determination of 0.66(10) (Masci et al., 2019). Contamination and spatial resolution differences cannot explain such a discrepancy between XANES and Mössbauer results because the chlorite crystals in this sample are clear and light-green colored (Ganzhorn et al., 2018). The contribution from magnetite in the Mössbauer data does not affect ferric iron determination, since its absorption does not overlap
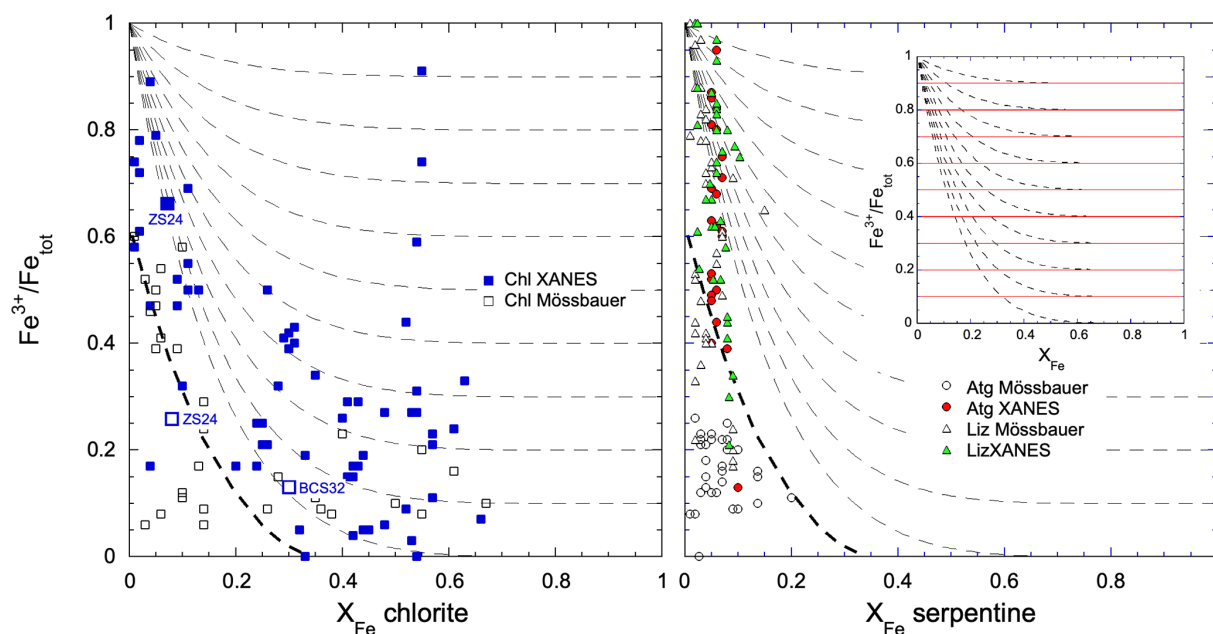
Figure 4. Fe^{3+} / Fe_{total} ratios from Mössbauer (open symbols) and XANES (filled symbols) measurements in chlorites (Chl) and serpentines (Atg: antigorite; Liz: lizardite) are reported as a function of X_{Fe}. Inset shows iso-values of the Fe^{3+} / Fe_{total} ratio in red, and the dashed curves show the corresponding Fe^{3+} / Fe_{total} ratio after photo-oxidation of isolated Fe^{2+} at low X_{Fe} (see text). Dashed curves after photo-oxidation are shown in all diagrams for comparison with XANES analyses. Photo-oxidation accounts semi-quantitatively for the higher Fe^{3+} / Fe_{total} ratio obtained by XANES on the Mg-rich side of the diagram. The thick dashed curve parallel to model curves is adjusted to the lowest XANES data on chlorites and reported at the same place on the serpentine diagram. It defines a field of low Fe^{3+} / Fe_{total} ratios where almost no XANES data on low-Fe chlorites and antigorites plot due to photo-oxidation, while Mössbauer data cover a large portion of it.

that of chlorite (Fig. 2, Table 2). Contamination of XANES by magnetite on the micrometer scale is unlikely because the XANES Fe^{3+} / Fe_{total} ratio of 0.66 would require total contamination by magnetite ($Fe^{2+}Fe_2^{3+}O_4$) on all six analyzed areas of the thin section (Masci et al., 2019).

Photo-oxidation of Mg-rich chlorites is suggested by the data that cover a larger X_{Fe} range (Fig. 4). All but one of the XANES analyses lie above a curve that is parallel to that of the minimum Fe^{3+} / Fe_{total} ratio predicted from the photo-oxidation model, suggesting that it is at least semi-quantitatively correct. The same line reported on the serpentine diagram also separates effectively the field of XANES analyses with the exception of 2 data points out of more than 60 (Fig. 4). Incomplete photo-oxidation in XANES may be due to partial recombination of defects or to partial ordering of Fe ions in the octahedral sites instead of the assumed complete disorder.

4.4 Mössbauer and XANES limitations

Conventional Mössbauer spectroscopy is not affected by photo-oxidation and alteration during the measurement, but it does not allow the precise mapping of Fe concentration and oxidation state provided by XANES. The latter method is essential for studying complex samples such as serpentinized

oceanic peridotites and their relationship to the production of reduced fluids (Andreani et al., 2013; Ellison et al., 2020) and complex and fine-grained extraterrestrial samples (Beck et al., 2012; Garenne et al., 2019). Synchrotron Mössbauer source (SMS) spectroscopy offers higher spatial resolution than conventional Mössbauer spectroscopy (Potapkin et al., 2012) and substantially less radiation flux than XANES; hence there is minimal risk of photo-oxidation (e.g., Gaborieau et al., 2020). However there are to this date fewer facilities that offer SMS compared to XANES.

The present model predicts that photo-oxidation is negligible when X_{Fe} is above about 0.2–0.3, in agreement with similar Mössbauer and XANES Fe^{3+} / Fe_{total} ratios in chlorites with X_{Fe} of ~ 0.2 (Fig. 4). XANES analysis of greenalite, a ferrous iron end-member serpentine of complex modulated structure (Guggenheim and Eggleton, 1998), yields pure Fe^{2+} (Beck et al., 2012), also suggesting negligible photo-oxidation in Fe-rich serpentine samples.

Interestingly, XANES results on Mg-rich talc and biotite (trioctahedral phlogopite) that contain only internal OH groups in TOT layers do not show such significant photo-oxidation as serpentines (Muñoz et al., 2013). This is consistent with the resistance of OH groups in natural talc to irradiation-induced H_2 production (Lainé et al., 2016) and with the absence of irradiation-induced iron oxidation in talc

and trioctahedral micas (Drago et al., 1977). It suggests that only phyllosilicates with external "brucite-like" OH such as serpentines and chlorites are prone to photo-oxidation, with a reaction of dehydrogenation that can be written as

$$2 \text{ "Fe}^{2+}(OH)_2\text{"} = 2 \text{ "Fe}^{3+}O(OH)\text{"} + H_2, \tag{3}$$
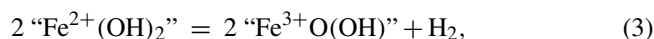
where "$Fe^{2+}(OH)_2$" and "$Fe^{3+}O(OH)$" refer to components in serpentine or chlorite. Thus photo-oxidation irreversibility may depend on efficient diffusion of hydrogen out of the crystals during irradiation.

Low Fe^{3+}/Fe_{total} ratios are observed by XANES in clinochlore single-crystals, of around 0.17 (Muñoz et al., 2013), and in one lizardite and one antigorite (Fig. 4), suggesting that other factors may influence photo-oxidation. A mixture with olivine could explain this observation because of the complex mineralogy of the natural samples (Andreani et al., 2013; Debret et al., 2014), but it is not possible in the case of the single-crystal study (Muñoz et al., 2013). Further XANES spectroscopic studies of well-characterized ferromagnesian phyllosilicates may help to elucidate these issues, as well as vibrational studies of OH bonds on XANES analytical spots. Well-characterized standards with similar composition and structure to the studied samples are necessary to improve the reliability of XANES mapping in Mg-rich phyllosilicates. For that purpose, the present samples are made available on demand to the scientific community.

5 Implications

Ferric iron determination influences phase equilibria modeling (Evans et al., 2012) because it is used to define the ferrous and ferric end-members of the lizardite, antigorite and chlorite solid solutions. Mg-rich terrestrial basic to ultrabasic compositions are not amenable to the use of XANES to determine accurate ferric iron contents in spite of the method's many advantages such as speed and spatial resolution, likely because of photo-oxidation. Nevertheless, XANES remains a reliable method for TOT phyllosilicates (talc and micas) and in terrestrial or extraterrestrial rocks with much higher iron contents (Beck et al., 2012; Garenne et al., 2019). Its application to Mg-rich serpentines and chlorite requires reevaluation and the use of well-characterized standards of the same mineralogical and compositional nature as the studied samples, instead of calibrations based on anhydrous compounds that are not significantly affected by photo-oxidation.

Mössbauer data are preferred over XANES data for estimating oxidation state budgets in hydrated mafic and ultramafic rocks of subduction zones (Evans, 2012; Mayhew and Ellison, 2020). Using the average ferric-to-total-iron ratios from Mössbauer data (Fig. 3) and modal mineralogies of high-pressure ultramafic rocks (Debret et al., 2014, 2015), the bulk ferric-to-total-iron ratios of the hydrated ultrabasic rocks change from 0.65(15) to 0.25(15) at the lizardite-to-antigorite transformation in Alpine ophiolites and from

0.4(1) to 0.15(5) at the antigorite–serpentinite-to-chlorite–harzburgite transition in Cerro del Almirez, at nearly constant bulk Fe content levels. This is to be compared to 0.70(15) to 0.50(15) and 0.55(5) to 0.15(5), respectively, using XANES data (Debret et al., 2014, 2015). The most important redox change is associated with the lizardite–antigorite transition occurring at 300–400 °C (Schwartz et al., 2013; Evans, 2004) rather than with the dehydration of antigorite occurring at 500–650 °C (Ulmer and Trommsdorff, 1995; Hilairet et al., 2006). With a large decrease in ferric iron and relatively small fluid release, the lizardite–antigorite transition is expected to release oxidized fluids in the cold mantle wedge. The major dehydration of antigorite is associated with a smaller decrease in ferric iron in the solid residue and should result in the release of large quantities of mildly oxidized fluids. The present estimates of Fe^{3+}/Fe_{total} ratios will affect the oxidation state of dehydration fluids in subduction zones (Debret and Sverjensky, 2017; Piccoli et al., 2019) and budgets of associated reactions affecting redox-sensitive elements such as carbon (Vitale Brovarone et al., 2017; Galvez et al., 2013). Continental alteration likely increases the Fe^{3+}/Fe_{total} ratio of hydrated ultramafic rocks, in agreement with conclusions reached from statistical analysis of available data (Mayhew and Ellison, 2020).

Review statement. This paper was edited by Giovanni B. Andreozzi and reviewed by three anonymous referees.

References

Aja, S. U. and Dyar, M. D.: The stability of Fe–Mg chlorites in hydrothermal solutions – I. Results of experimental investigations, Appl. Geochem., 17, 1219–1239, https://doi.org/10.1016/S0883-2927(01)00131-7, 2002.

Andreani, M., Muñoz, M., Marcaillou, C., and Delacour, A.: μ-XANES study of iron redox state in serpentine during oceanic serpentinization, Lithos, 178, 70–83, https://doi.org/10.1016/j.lithos.2013.04.008, 2013.

Beck, P., De Andrade, V., Orthous-Daunay, F. R., Veronesi, G., Cotte, M., Quirico, E., and Schmitt, B.: The redox state of iron in the matrix of CI, CM and metamorphosed CM chondrites by XANES spectroscopy, Geochim. Cosmochim. Ac., 99, 305–316, https://doi.org/10.1016/j.gca.2012.04.041, 2012.

Bertoldi, C., Benisek, A., Cemic, L., and Dachs, E.: The heat capacity of two natural chlorite group minerals derived from differential scanning calorimetry, Phys. Chem. Mineral., 28, 332–336, https://doi.org/10.1007/s002690100157, 2001.

Billault, V., Beaufort, D., Patrier, P., and Petit, S.: Crystal chemistry of Fe-sudoites from uranium deposits in the Athabasca Basin (Saskatchewan, Canada), Clay. Clay Mineral., 50, 70–81, 2002.

Chernosky, J. V., Berman, R. G., and Bryndzia, L. T.: Stability, phase relations, and thermodynamic properties of chlorite and serpentine group minerals, Rev. Mineral. Geochem., 19, 295–346, 1988.

Cottrell, E., Lanzirotti, A., Mysen, B., Birner, S., Kelley, K. A., Botcharnikov, R., Davis, F. A., and Newville, M.: A Mössbauer-based XANES calibration for hydrous basalt glasses reveals radiation-induced oxidation of Fe, Am. Mineral., 103, 489–501, https://doi.org/10.2138/am-2018-6268, 2018.

Debret, B. and Sverjensky, D.: Highly oxidising fluids generated during serpentinite breakdown in subduction zones, Sci. Rep., 7, 10351, https://doi.org/10.1038/s41598-017-09626-y, 2017.

Debret, B., Andreani, M., Munoz, M., Bolfan-Casanova, N., Carlut, J., Nicollet, C., Schwartz, S., and Trcera, N.: Evolution of Fe redox state in serpentine during subduction, Earth Planet. Sc. Lett., 400, 206–218, https://doi.org/10.1016/j.epsl.2014.05.038, 2014.

Debret, B., Bolfan-Casanova, N., Padron-Navarta, J. A., Martin-Hernandez, F., Andreani, M., Garrido, C. J., Sanchez-Vizcaino, V. L., Gomez-Pugnaire, M. T., Munoz, M., and Trcera, N.: Redox state of iron during high-pressure serpentinite dehydration, Contrib. Mineral. Petr., 169, 36, https://doi.org/10.1007/s00410-015-1130-y, 2015.

De Grave, E., Vandenbruwaene, J., and Van Bockstael, M.: 57Fe Mössbauer spectroscopic analysis of chlorite, Phys. Chem. Mineral., 15, 173–180, https://doi.org/10.1007/bf00308781, 1987.

Drago, V., Baggio Saitovitch, E., and Danon, J.: Mössbauer spectroscopy of electron irradiated natural layered silicates, J. Inorg. Nucl. Chem., 39, 973–979, https://doi.org/10.1016/0022-1902(77)80246-7, 1977.

Dyar, M. D., Gunter, M. E., Delaney, J. S., Lanzarotti, A., and Sutton, S. R.: Systematics in the structure and XANES spectra of pyroxenes, amphiboles, and micas as derived from oriented single crystals, Can. Mineral., 40, 1375–1393, https://doi.org/10.2113/gscanmin.40.5.1375, 2002.

Ehlmann, B. L., Mustard, J. F., Swayze, G. A., Clark, R. N., Bishop, J. L., Poulet, F., Marais, D. J. D., Roach, L. H., Milliken, R. E., Wray, J. J., Barnouin-Jha, O., and Murchie, S. L.: Identification of hydrated silicate minerals on Mars using MRO-CRISM: Geologic context near Nili Fossae and implications for aqueous alteration, J. Geophys. Res.-Planet., 114, E00d08, https://doi.org/10.1029/2009je003339, 2009.

Ellison, E. T., Mayhew, L. E., Miller, H. M., and Templeton, A. S.: Quantitative microscale Fe redox imaging by multiple energy X-ray fluorescence mapping at the Fe K pre-edge peak, Am. Mineral., 105, 1812–1829, https://doi.org/10.2138/am-2020-7359, 2020.

Etiope, G., Schoell, M., and Hosgormez, H.: Abiotic methane flux from the Chimaera seep and Tekirova ophiolites (Turkey): Understanding gas exhalation from low temperature serpentinization and implications for Mars, Earth Planet. Sc. Lett., 310, 96–104, https://doi.org/10.1016/j.epsl.2011.08.001, 2011.

Evans, B. W.: The serpentinite multisystem revisited: Chrysotile is metastable, Int. Geol. Rev., 46, 479–506, 2004.

Evans, B. W., Dyar, M. D., and Kuehner, S. M.: Implications of ferrous and ferric iron in antigorite, Am. Mineral., 97, 184–196, 2012.

Evans, K. A.: The redox budget of subduction zones, Earth-Sci. Rev., 113, 11–32, https://doi.org/10.1016/j.earscirev.2012.03.003, 2012.

Fruh-Green, G. L., Connolly, J. A. D., Plas, A., Kelley, D. S., and Grobety, B.: Serpentinization of oceanic peridotites: Implications for geochemical cycles and biological activity, in: Subseafloor Biosphere at Mid-Ocean Ranges, edited by: Wilcock, W. S. D., DeLong, E. F., Kelley, D. S., Baross, J. A., and Cary, S. C., Geophys. Monogr. Ser., 144, 119–136, https://doi.org/10.1029/144gm08, 2004.

Fuchs, Y., Linares, J., and Mellini, M.: Mössbauer and infrared spectroscopy of lizardite-1T from Monte Fico, Elba, Phys. Chem. Mineral., 26, 111–115, 1998.

Gaborieau, M., Laubier, M., Bolfan-Casanova, N., McCammon, C. A., Vantelon, D., Chumakov, A. I., Schiavi, F., Neuville, D. R., and Venugopal, S.: Determination of $Fe^{3+}/\Sigma Fe$ of olivine-hosted melt inclusions using Mössbauer and XANES spectroscopy, Chem. Geol., 547, 119646, https://doi.org/10.1016/j.chemgeo.2020.119646, 2020.

Galvez, M. E., Beyssac, O., Martinez, I., Benzerara, K., Chaduteau, C., Malvoisin, B., and Malavieille, J.: Graphite formation by carbonate reduction during subduction, Nat. Geosci., 6, 473–477, https://doi.org/10.1038/ngeo1827, 2013.

Ganzhorn, A.-C., Pilorgé, H., Le Floch, S., Montagnac, G., Cardon, H., and Reynard, B.: Deuterium-hydrogen

inter-diffusion in chlorite, Chem. Geol., 493, 518–524, https://doi.org/10.1016/j.chemgeo.2018.07.010, 2018.

Garenne, A., Beck, P., Montes-Hernandez, G., Bonal, L., Quirico, E., Proux, O., and Hazemann, J. L.: The iron record of asteroidal processes in carbonaceous chondrites, Meteorit. Planet. Sci., 54, 2652–2665, https://doi.org/10.1111/maps.13377, 2019.

Goodman, B. A. and Bain, D. C.: Mössbauer Spectra of Chlorites and Their Decomposition Products, in: Developments in Sedimentology, edited by: Mortland, M. M. and Farmer, V. C., Elsevier, 65–74, https://doi.org/10.1016/S0070-4571(08)70702-7, 1979.

Gregori, D. A. and Mercader, R. C.: Mössbauer study of some Argentinian chlorites, Hyperfine Interact., 83, 495–498, https://doi.org/10.1007/BF02074324, 1994.

Guggenheim, S. and Eggleton, R. A.: Modulated crystal structures of greenalite and caryopilite; a system with long-range, in-plane structural disorder in the tetrahedra sheet, Can. Mineral., 36, 163–179, 1998.

Hilairet, N., Daniel, I., and Reynard, B.: Equation of state of antigorite, stability field of serpentines, and seismicity in subduction zones, Geophys. Res. Lett., 33, L02302, https://doi.org/10.1029/2005GL024728, 2006.

Kelley, D. S., Karson, J. A., Blackman, D. K., Fruh-Green, G. L., Butterfield, D. A., Lilley, M. D., Olson, E. J., Schrenk, M. O., Roe, K. K., Lebon, G. T., Rivizzigno, P., and Party, A. T. S.: An off-axis hydrothermal vent field near the Mid-Atlantic Ridge at 30° N, Nature, 412, 145–149, https://doi.org/10.1038/35084000, 2001.

Lainé, M., Allard, T., Balan, E., Martin, F., Von Bardeleben, H. J., Robert, J.-L., and Caër, S. L.: Reaction Mechanisms in Talc under Ionizing Radiation: Evidence of a High Stability of H Atoms, J. Phys. Chem. C, 120, 2087–2095, https://doi.org/10.1021/acs.jpcc.5b11396, 2016.

Lougear, A., Grodzicki, M., Bertoldi, C., Trautwein, A. X., Steiner, K., and Amthauer, G.: Mössbauer and molecular orbital study of chlorites, Phys. Chem. Mineral., 27, 258–269, https://doi.org/10.1007/s002690050255, 2000.

Malmström, M., Banwart, S., Lewenhagen, J., Duro, L., and Bruno, J.: The dissolution of biotite and chlorite at 25 °C in the near-neutral pH region, J. Contamin. Hydrol., 21, 201–213, https://doi.org/10.1016/0169-7722(95)00047-X, 1996.

Masci, L., Dubacq, B., Verlaguet, A., Chopin, C., De Andrade, V., and Herviou, C.: A XANES and EPMA study of Fe^{3+} in chlorite: Importance of oxychlorite and implications for cation site distribution and thermobarometry, Am. Mineral., 104, 403–417, https://doi.org/10.2138/am-2019-6766, 2019.

Mayhew, L. E. and Ellison, E. T.: A synthesis and meta-analysis of the Fe chemistry of serpentinites and serpentine minerals, Philos. T. R. Soc. A, 378, 20180420, https://doi.org/10.1098/rsta.2018.0420, 2020.

McCammon, C. A., Chaskar, V., and Richards, G. G.: A technique for spatially Mössbauer spectroscopy applied to quenched metallurgical slags, Meas. Sci. Technol., 2, 657–662, 1991.

Mellini, M., Fuchs, Y., Viti, C., Lemaire, C., and Linarès, J.: Insights into the antigorite structure from Mössbauer and FTIR spectroscopies, Europ. J. Mineral., 14, 97–104, 2002.

Mitra, S. and Bidyananda, M.: Crystallo-chemical characteristics of chlorites from the greenstone belt of South India, and their geothermometric significance, Clay Sci., 11, 479–501, https://doi.org/10.11362/jcssjclayscience1960.11.479, 2001.

Moore, T.: Petrology and tectonic implications of the blueschist-bearing Puerto Nuevo melange complex, Vizcaino Peninsula, Baja California Sur, Mexico, Geol. Soc. Am. Memoir, 164, 43–58, 1986.

Muir, I. J., Metson, J. B., and Bancroft, G. M.: [57]Fe Moessbauer spectra of perovskite and titanite, Can. Mineral., 22, 689–694, 1984.

Muñoz, M., De Andrade, V., Vidal, O., Lewin, E., Pascarelli, S., and Susini, J.: Redox and speciation micromapping using dispersive X-ray absorption spectroscopy: Application to iron in chlorite mineral of a metamorphic rock thin section, Geochem. Geophy. Geosy., 7, Q11020, https://doi.org/10.1029/2006GC001381, 2006.

Muñoz, M., Vidal, O., Marcaillou, C., Pascarelli, S., Mathon, O., and Farges, F.: Iron oxidation state in phyllosilicate single crystals using Fe-K pre-edge and XANES spectroscopy: Effects of the linear polarization of the synchrotron X-ray beam, Am. Mineral., 98, 1187–1197, https://doi.org/10.2138/am.2013.4289, 2013.

O'Hanley, D. S. and Dyar, M. D.: The composition of lizardite 1T and the formation of magnetite in serpentinites, Am. Mineral., 78, 391–404, 1993.

O'Hanley, D. S. and Dyar, M. D.: The composition of chrysotile and its relationship with lizardite, Can. Mineral., 36, 727–739, 1998.

Padrón-Navarta, J. A., López Sánchez-Vizcaíno, V., Garrido, C. J., and Gómez-Pugnaire, M. T.: Metamorphic Record of High-pressure Dehydration of Antigorite Serpentinite to Chlorite Harzburgite in a Subduction Setting (Cerro del Almirez, Nevado–Filábride Complex, Southern Spain), J. Petrol., 52, 2047–2078, https://doi.org/10.1093/petrology/egr039, 2011.

Peretti, A., Dubessy, J., Mullis, J., Frost, B. R., and Trommsdorff, V.: Highly reducing conditions during Alpine metamorphism of the Malenco peridotite (Sondrio, northern Italy) indicated by mineral paragenesis and H_2 in fluid inclusions, Contrib. Mineral. Petr., 112, 329–340, https://doi.org/10.1007/BF00310464, 1992.

Piccoli, F., Hermann, J., Pettke, T., Connolly, J. A. D., Kempf, E. D., and Vieira Duarte, J. F.: Subducting serpentinites release reduced, not oxidized, aqueous fluids, Sci. Rep., 9, 19573, https://doi.org/10.1038/s41598-019-55944-8, 2019.

Piilonen, P. C., Rancourt, D. G., Evans, R. J., Lalonde, A. E., McDonald, A. M., and Shabani, A. A. T.: The relationships between crystal-chemical and hyperfine parameters in members of the astrophyllite-group: A combined[57]Fe Mossbauer spectroscopy and single-crystal X-ray diffraction study, European J. Mineral., 16, 989–1002, https://doi.org/10.1127/0935-1221/2004/0016-0989, 2004.

Pons, M., Quitté, G., Fujii, T., Rosing, M., Reynard, B., Moynier, F., Douchet, C., and Albarède, F.: Early Archean serpentine mud volcanoes at Isua, Greenland, as a niche for early life, P. Natl. Acad. Sci. USA, 108, 17639–17643, https://doi.org/10.1073/pnas.1108061108, 2011.

Potapkin, V., Chumakov, A. I., Smirnov, G. V., Celse, J.-P., Ruffer, R., McCammon, C., and Dubrovinsky, L.: The 57Fe Synchrotron Mossbauer Source at the ESRF, J. Synchrot. Rad., 19, 559–569, https://doi.org/10.1107/S0909049512015579, 2012.

Prescher, C., McCammon, C., and Dubrovinsky, L.: MossA: a program for analyzing energy-domain Mossbauer spectra from con-

ventional and synchrotron sources, J. Appl. Crystallogr., 45, 329–331, https://doi.org/10.1107/S0021889812004979, 2012.

Rancourt, D. G.: Mössbauer spectroscopy of minerals, Phys. Chem. Mineral., 21, 244–249, https://doi.org/10.1007/BF00202138, 1994.

Reynard, B., Mibe, K., and Van de Moortele, B.: Electrical conductivity of the serpentinised mantle and fluid flow in subduction zones, Earth Planet. Sc. Lett., 307, 387–394, https://doi.org/10.1016/j.epsl.2011.05.013, 2011.

Reynard, B., Bezacier, L., and Caracas, R.: Serpentines, talc, chlorites, and their high-pressure phase transitions: a Raman spectroscopic study, Phys. Chem. Mineral., 42, 641–649, 10.1007/s00269-015-0750-0, 2015.

Rigault, C.: Cristallochimie du fer dans les chlorites de basse température: implications pour la géothermométrie et la détermination des paléoconditions redox dans les gisements d'uranium, Université de Poitiers, France, 280 pp., 2010.

Rozenson, I., Bauminger, E., and Heller-Kallai, L.: Mössbauer spectra of iron in 1 : 1 phyllosilicate, Am. Mineral., 64, 893–901, 1979.

Scambelluri, M., Piccardo, G. B., Philippot, P., Robbiano, A., and Negretti, L.: High salinity fluid inclusions formed from recycled seawater in deeply subducted alpine serpentinite, Earth Planet. Sc. Lett., 148, 485–499, 1997.

Schulte, M., Blake, D., Hoehler, T., and McCollom, T.: Serpentinization and its implications for life on the early Earth and Mars, Astrobiology, 6, 364–376, https://doi.org/10.1089/ast.2006.6.364, 2006.

Schwartz, S., Guillot, S., Reynard, B., Lafay, R., Debret, B., Nicollet, C., Lanari, P., and Auzende, A. L.: Pressure-temperature estimates of the lizardite/antigorite transition in high pressure serpentinites, Lithos, 178, 197–210, https://doi.org/10.1016/j.lithos.2012.11.023, 2013.

Sedlock, R. L.: Four phases of Mesozoic deformation in the Sierra de San Andres Ophiolite, Vizcaíno Peninsula, west-central Baja California, México, in: Tectonic evolution of northwestern Mexico and the Southwestern USA, edited by: Johnson, S. E., Paterson, S. R., Fletcher, J. M., Girty, G. H., Kimbrough, D. L., and Martín-Barajas, A., Geological Society of America, https://doi.org/10.1130/0-8137-2374-4.73, 2003.

Smyth, J. R., Dyar, M. D., May, H. M., Bricker, O. P., and Acker, J. G.: Crystal Structure Refinement and Mössbauer Spectroscopy of an Ordered, Triclinic Clinochlore, Clay. Clay Mineral., 45, 544–550, https://doi.org/10.1346/CCMN.1997.0450406, 1997.

Sobolev, V. N., McCammon, C. A., Taylor, L. A., Snyder, G. A., and Sobolev, N. V.: Precise Moessbauer milliprobe determination of ferric iron in rock-forming minerals and limitations of electron microprobe analysis, Am. Mineral., 84, 78–85, https://doi.org/10.2138/am-1999-1-208, 1999.

Steven, C., Dyar, M. D., McCanta, M., Newville, M., and Lanzirotti, A.: Wave vector and field vector orientation dependence of Fe K pre-edge X-ray absorption features in clinopyroxenes, Am. Mineral., https://doi.org/10.2138/am-2022-8547, 2022.

Trincal, V., Lanari, P., Buatier, M., Lacroix, B., Charpentier, D., Labaume, P., and Muñoz, M.: Temperature micro-mapping in oscillatory-zoned chlorite: Application to study of a green-schist facies fault zone in the Pyrenean Axial Zone (Spain), Am. Mineral., 100, 2468–2483, https://doi.org/10.2138/am-2015-5217, 2015.

Tsujimori, T. and Itaya, T.: Blueschist-facies metamorphism during Paleozoic orogeny in southwestern Japan: Phengite K–Ar ages of blueschist-facies tectonic blocks in a serpentinite melange beneath early Paleozoic Oeyama ophiolite, Island Arc, 8, 190–205, 1999.

Ulmer, P. and Trommsdorff, V.: Serpentine Stability to Mantle Depths and Subduction-Related Magmatism, Science, 268, 858–861, https://doi.org/10.1126/science.268.5212.858, 1995.

Vidal, O., De Andrade, V., Lewin, E., Munoz, M., Parra, T., and Pascarelli, S.: P–T-deformation-Fe^{3+} / Fe^{2+} mapping at the thin section scale and comparison with XANES mapping: application to a garnet-bearing metapelite from the Sambagawa metamorphic belt (Japan), J. Metamor. Geol., 24, 669–683, https://doi.org/10.1111/j.1525-1314.2006.00661.x, 2006.

Vitale Brovarone, A., Martinez, I., Elmaleh, A., Compagnoni, R., Chaduteau, C., Ferraris, C., and Esteve, I.: Massive production of abiotic methane during subduction evidenced in metamorphosed ophicarbonates from the Italian Alps, Nat. Commun., 8, 14134, https://doi.org/10.1038/ncomms14134, 2017.

Vitale Brovarone, A., Sverjensky, D. A., Piccoli, F., Ressico, F., Giovannelli, D., and Daniel, I.: Subduction hides high-pressure sources of energy that may feed the deep subsurface biosphere, Nat. Commun., 11, 3880, https://doi.org/10.1038/s41467-020-17342-x, 2020.

Votyakov, S. L., Chaschukhin, I. S., Galakhova, O. L., and Gulyaeva, T. Y.: Crystal chemistry of lizardite as an indicator of early serpentinization in ultramafic rocks, I. Compositional and structural features of the mineral according to spectroscopic data, Geochem. Int., 43, 862–880, 2005.

Wilke, M., Farges, F., Petit, P. E., Brown, G. E., and Martin, F.: Oxidation state and coordination of Fe in minerals: a Fe-XANES spectroscopic study, Am. Mineral., 86, 714–730, 2001.

Zazzi, Å., Hirsch, T. K., Leonova, E., Kaikkonen, A., Grins, J., Annersten, H., and Edèin, M.: Structural investigations of natural and synthetic chlorite minerals by X-ray diffraction, Mössbauer spectropscopy and solid-state nuclear magnetic resonance, Clay. Clay Mineral., 54, 252–265, https://doi.org/10.1346/CCMN.2006.0540210, 2006.